Manuscript Details

Manuscript number	JCOMB_2018_2071
Title	THE EFFECTS OF ELEVATED TEMPERATURE ON THE BOND BEHAVIOUR OF SAND COATED GFRP BARS TO CONCRETE – DEFINITION OF BOND vs. SLIP RELATIONS
Article type	Full Length Article

Abstract

The use of glass fibre reinforced polymer (GFRP) bars as internal reinforcement of new and existing (for rehabilitation or retrofitting) concrete structures has been growing, mainly due to the advantages they present over traditional steel reinforcement, namely their low weight, high strength and corrosion resistance. However, at moderately elevated temperatures, especially when approaching the glass transition temperature (Tg) of the polymeric matrix (usually between 65-150 ºC), the stiffness, strength and bond properties of these rebars are known to be significantly degraded. The first part of this paper presents an experimental investigation comprising tensile and pull-out tests on sand coated GFRP rebars at elevated temperatures; the tensile tests were carried out up to 300 ºC, whereas the pull-out tests were performed on GFRP rebars embedded in concrete cylinders at 20 ºC, 40 ºC, 60 ºC, 80 ºC, 100 ºC and 140 ºC; two embedment lengths of the rebars were considered, corresponding to 5 and 9 times their diameter. Specimens were first heated up to the predefined temperature (measured at the GFRP-concrete interface) and then loaded up to failure. The applied load and the slip of the rebars at both loaded and free ends were measured during the pull-out tests. The obtained results confirmed that the stiffness and strength of the GFRP-concrete interface are significantly reduced with temperature increase, especially when the Tg of the GFRP rebars is approached and exceeded. In the second part of the paper, analytical bond vs. slip relations for the GFRP-concrete interface are proposed for each of the tested temperatures; these relations were obtained based on a numerical strategy in which the experimental data from the pull-out tests were used to calibrate the defining parameters of the local bond vs. slip laws. Moreover, the accuracy of two empirical (relaxation) models, proposed by Gibson et al. and Correia et al. in predicting the GFRP-concrete bond strength reduction with temperature was also assessed.

Keywords	A. Glass fibres; B. Adhesion; B. High-temperature properties; D. Mechanical testing
Manuscript region of origin	Europe
Corresponding Author	João Pedro Firmo
Corresponding Author's Institution	CEris - CIVIL ENGINEERING RESEARCH AND INNOVATION FOR SUSTAINABILITY
Order of Authors	Inês Rosa, João Pedro Firmo, Joao Correia, Joaquim Barros
Suggested reviewers	antonio bilotta, Mark Green, Luke Bisby

Submission Files Included in this PDF

File Name [File Type]

Firmo&al-CoverLetter.docx [Cover Letter]

manuscript_bond sand coated_FINAL_no links.pdf [Manuscript File]

To view all the submission files, including those not included in the PDF, click on the manuscript title on your EVISE Homepage, then click 'Download zip file'.

Lisbon, 11th July 2018

To whom it may concern,

Attached, please find the paper "*The effects of elevated temperature on the bond behaviour of sand coated GFRP bars to concrete – definition of bond vs. slip relations*" by Inês C. Rosa, João P. Firmo, João R. Correia and Joaquim A. O. Barros that we wish to submit for publication in the *Composites Part B: Engineering* journal.

I hereby confirm that the research presented in the paper is original and has not been published before or submitted for publication elsewhere. I also confirm that the submission has been approved by all co-authors.

Please let me know if you need any additional elements and feel free to contact me at any time for any comment or question you would judge useful for the review.

Yours sincerely,

João Pedro Firmo

João Pedro Firmo

João Pedro Firmo
Research Assistant
Instituto Superior Técnico, Universidade de Lisboa
Department of Civil Engineering, Architecture and Georesources
Av. Rovisco Pais, 1049-001 Lisboa, Portugal
Phone: +351 2184188240
Fax: +351 218418276
Email: joao.firmo@técnico.ulisboa.pt

THE EFFECTS OF ELEVATED TEMPERATURE ON THE BOND BEHAVIOUR OF SAND COATED GFRP BARS TO CONCRETE – DEFINITION OF BOND *vs.* SLIP RELATIONS

I. C. Rosa[a], J. P. Firmo[b], J. R. Correia[c], J. A. O. Barros[d]

[a] CERIS, Instituto Superior Técnico, Universidade de Lisboa, Av. Rovisco Pais 1, 1049-001 Lisboa, Portugal; ines.rosa@tecnico.ulisboa.pt

[b] CERIS, Instituto Superior Técnico, Universidade de Lisboa, Av. Rovisco Pais 1, 1049-001 Lisboa, Portugal; joao.firmo@tecnico.ulisboa.pt

[c] CERIS, Instituto Superior Técnico, Universidade de Lisboa, Av. Rovisco Pais 1, 1049-001 Lisboa, Portugal; joao.ramoa.correia@tecnico.ulisboa.pt

[d] ISISE, Universidade do Minho, Campus de Azurém, 4800 Guimarães, Portugal; barros@civil.uminho.pt

Abstract: The use of glass fibre reinforced polymer (GFRP) bars as internal reinforcement of new and existing (for rehabilitation or retrofitting) concrete structures has been growing, mainly due to the advantages they present over traditional steel reinforcement, namely their low weight, high strength and corrosion resistance. However, at moderately elevated temperatures, especially when approaching the glass transition temperature (T_g) of the polymeric matrix (usually between 65-150 ℃), the stiffness, strength and bond properties of these rebars are known to be significantly degraded. The first part of this paper presents an experimental investigation comprising tensile and pull-out tests on sand coated GFRP rebars at elevated temperatures; the tensile tests were carried out up to 300 ℃, whereas the pull-out tests were performed on GFRP rebars embedded in concrete cylinders at 20 ℃, 40 ℃, 60 ℃, 80 ℃, 100 ℃ and 140 ℃; two embedment lengths of the rebars were considered, corresponding to 5 and 9 times their diameter. Specimens were first heated up to the predefined temperature (measured at the GFRP-concrete interface) and then loaded up to failure. The applied load and the slip of the rebars at both loaded and free ends were measured during the pull-out tests. The obtained results confirmed that the stiffness and strength of the GFRP-concrete interface are significantly reduced with temperature increase, especially when the T_g of the GFRP rebars is approached and exceeded. In the second part of the paper, analytical bond *vs.* slip relations for the GFRP-concrete interface are proposed for each of the tested temperatures; these relations were obtained based on a numerical strategy in which the experimental data from the pull-out tests were used to calibrate the defining parameters of the local bond *vs.* slip laws. Moreover, the accuracy of two empirical (relaxation) models, proposed by Gibson *et al.* and Correia *et al.* in predicting the GFRP-concrete bond strength reduction with temperature was also assessed.

Keywords: A. Glass fibres; B. Adhesion; B. High-temperature properties; D. Mechanical testing.

1 INTRODUCTION

36 The corrosion of steel reinforcement is one of the main factors that contribute to the degradation

37 of reinforced concrete (RC) structures, being particularly relevant in highly aggressive

38 environments, such as under exposure to seawater and de-icing salts (*e.g.,* in maritime structures

39 or bridge decks, respectively) or chemical and radioactive wastes (*e.g.*, in industrial facilities) [1].

40 To overcome this challenge, glass fibre reinforced polymer (GFRP) rebars are being used as a

41 non-corrodible alternative to the traditional steel reinforcement [2, 3]. These composite materials

42 are not only lighter than steel, but they also have higher tensile strength, electromagnetic

43 transparency and present low maintenance requirements [4]. Presently, their applications extend

44 from new construction to the rehabilitation of degraded RC structures (*e.g.*, as a replacement for

45 corroded steel rebars).

46 One of the main issues concerning the use of GFRP rebars is their behaviour at elevated

47 temperature and under fire exposure. In fact, their mechanical properties, namely the tensile

48 strength and the elastic modulus, are known to experience significant reductions, especially when

49 approaching the glass transition temperature (T_g) of the polymeric matrix (usually between

50 65-150 °C [5]). Despite its relevance, the fire performance of GFRP materials and GFRP-RC

51 structures is still not comprehensively addressed in the literature, which explains why most design

52 guidelines (conservatively) do not recommend yet the use of GFRP rebars in structures where the

53 fire action has to be considered at design (*i.e.*, in buildings) [4, 6].

54 The concerns about the use of GFRP rebars in structures likely to be subjected to elevated service

55 temperatures and/or fire also encompass the degradation of their bond behaviour to concrete. In

56 fact, elevated temperature has been referred to play an important role on the deterioration of the

57 bond capacity of GFRP rebars in concrete [7, 8]. This is particularly worrying, even for

58 moderately elevated temperatures; indeed, several authors (*e.g.*, [9, 10]) have reported premature

59 structural collapses of GFRP-RC slabs exposed to fire due to rebars' debonding in lap-slices.

60   This paper presents experimental and analytical investigations on the effects of moderately elevated

61   temperatures on the bond between sand coated GFRP rebars and concrete. The experiments

62   described in sections 3 and 4 include (i) tensile tests on the GFRP rebars, from ambient temperature

63   up to 300 ℃, and (ii) pull-out tests on GFRP rebars embedded in concrete cylinders, with two

64   different embedment lengths, from ambient temperature up to 140 ℃. The analytical studies,

65   presented in section 5, include: (i) the development of temperature-dependent bond stress *vs.* slip

66   models, and (ii) the assessment of the accuracy of two empirical models, described in the literature,

67   for modelling the effect of temperature on the bond strength.

68   **2   LITERATURE REVIEW**

69   Over the last two decades, a considerable number of investigations has contributed to improve

70   the understanding of the bond behaviour between FRP rebars and concrete at ambient

71   temperature. The studies available in the literature have demonstrated that the FRP-concrete

72   interaction depends on parameters such as the material type of FRP reinforcement, the roughness

73   of the bar's surface, the bar diameter, the embedment length, the bar end geometry, the concrete

74   strength, the concrete cover, the confinement pressure, the position of the rebar w.r.t. the direction

75   of casting (top-bar effect), as well as on environmental conditions (*e.g.*, [11]). However,

76   investigations performed on the FRP-concrete bond behaviour at elevated temperatures are still

77   relatively scarce; moreover, as highlighted next, bond stress *vs.* slip laws describing the FRP-

78   concrete interaction at elevated temperatures have not yet comprehensively developed. Such laws

79   are needed to accurately simulate the behaviour at elevated temperature and under fire exposure

80   of GFRP-RC members.

81   Katz *et al.* [7] performed pull-out tests on steel and GFRP rebars with different surface finishing

82   (large surface deformations and helical fibre wrap combined with sand coating and/or surface

83   deformations); the T_gs of the GFRP rebars ranged from 60 ℃ to 124 ℃ (the test methods used to

84   determine the T_gs were not specified). The steel/GFRP-concrete specimens, with an embedment

85   length of the rebars in concrete of 5 diameters, were heated from ambient temperature (20 ℃) up

3

86   to 250-350 ℃. The authors concluded that the bond performance at ambient temperature, as well

87   as the bond strength and stiffness degradation with temperature, depend mostly on parameters

88   associated with the surface properties of the rebars. At ambient temperature, bond strength values

89   obtained in most GFRP rebars were higher (6 to 37% more) than those obtained for the steel

90   rebars; higher bond strengths were attained in rebars with large surface deformations (*i.e.*,

91   moulded indentations resembling steel surface deformations) and rebars with wrapped fibres

92   combined with fine sand particles embedded in the rebars' surface. Similar reductions of bond

93   strength with temperature were obtained for all GFRP rebars tested. Most part of the bond strength

94   reduction occurred for temperatures below 180-200 ℃, being particularly pronounced below and

95   during the glass transition. At 200 ℃, the GFRP bond strength was reduced at least 80%

96   (compared to that measured at ambient temperature), while in the steel rebars, at the same

97   temperature, that reduction was only 38%; above 200 ℃, the GFRP bond strength did not exhibit

98   significant further reductions with temperature. These reductions were considerably higher than

99   those obtained for the steel rebars, in which the bond strength reduction at 210 ℃ was about 34%.

100   The bond stiffness reduction was fairly similar for GFRP and steel rebars; the rebars with wrapped

101   fibres combined with a sand coating performed slightly better than the remaining GFRP rebars,

102   presenting a stiffness reduction of 39% at 230 ℃.

103   McIntyre *et al.* [12] studied the GFRP-concrete bond performance from 25 ℃ and 150 ℃ of

104   GFRP rebars with two types of surface finishing: a thin sand coating associated with a double

105   helical fibre wrap (BPG rebar) and a coarse sand coating (PTG rebar). The diameter of the rebars

106   were 10 mm and 9.5 mm and their T_gs (determined from the onset of the storage modulus) were

107   86 ℃ and 84 ℃, respectively for the BPG and PTG rebar. The embedment length of the rebars in

108   concrete was approximately 4 times the diameter of the rebars. A steep reduction of the bond

109   strength occurred for temperatures below the corresponding T_gs: at those temperatures, strength

110   retentions were about 54% and 44% (compared to the bond strength at 25 ℃), for the BPG and

111   PTG rebars, respectively. At 150 ℃, bond strength retentions were 37% for the BPG rebar and

112   only 18% for the PTG rebar. It should be noted that the vast majority of the specimens exhibited

113   splitting failure, instead of the desired pull-out failure, preventing the determination of the actual

114   bond strength reductions with temperature for those specimens.

115   Calvet *et al.* [13] studied the effect of exposing different CFRP and steel rebars to various

116   environments (from 5 ℃ to 80 ℃) on their bond behaviour to concrete. The CFRP rebars differed

117   on the surface finishing (sand coated, ribbed, deformed and textured) and on the diameter (8 mm

118   or 14 mm); the embedment length in concrete was 5 times the diameter of the rebars, and their T_g

119   (determined through differential scanning calorimetry experiments) varied between 105 ℃ to

120   123 ℃. Pull-out tests in sand coated CFRP rebars with diameters of 8 mm and 14 mm showed

121   maximum bond strength reductions at 80 ℃ (compared to those at 20 ℃) of 34% and 19%,

122   respectively. This study also showed that at 80℃ (below the T_g of the rebars) the bond strength

123   reduction was higher in the ribbed (CFRP) rebars than in the deformed and sand coated rebars

124   (39% *vs.* 16-19% reduction); the bond strength reductions experienced by the last two types of

125   rebars were in fact very similar to that obtained in the ribbed steel rebars (21%). Splitting failure

126   modes were not reported.

127   The study of Chenchen *et al.* [14] focused on the influence of several parameters in the residual

128   behaviour of the FRP-concrete interface (*i.e.* after exposure to elevated temperature followed by

129   cooling to ambient temperature), namely: (i) the type of fibre reinforcement (GFRP or BFRP),

130   (ii) the embedment length (2.5*d*, 5*d*, 10*d*, 15*d* and 20*d*, where *d* is the diameter of the rebar), (iii) the

131   rebars' diameter (6, 8 and 10 mm), (iv) the concrete strength (grades C30, C45 and C60), and (v)

132   the thickness of the concrete cover (3*d*, 6*d* and 9*d*). Regarding the influence of the type of fibre

133   reinforcement, the authors tested 8 mm GFRP and BFRP rebars embedded in concrete cubes with

134   an embedment length of 5*d*. Both rebars had a helical wrapping surface (the BFRP rebars also had

135   a superficial sand coating). The pull-out specimens were previously heated up to a maximum

136   temperature of 350 ℃ and then tested after being cooled down to ambient temperature. After

137   exposure to 220 ℃, the bond strength reductions (compared to those at ambient temperature) were

138   7% and 14% for the BFRP and GFRP specimens, respectively; for 270 ℃, those reductions

139   progressed to 32% in both types of rebars, and for 350 ℃, the bond strength presented a severe

140   reduction of 88% and 77% for the BFRP and GFRP rebars, respectively (the failure mode of most

141   tested specimens was by pull-out). The influence of the embedment length, rebar diameter, concrete

142   strength and concrete cover thickness was assessed for the BFRP rebars. As expected, at both

143   ambient temperature and elevated temperature, the average bond strength decreased with the

144   embedment length and bar diameter and it increased with the concrete strength and cover thickness.

145   Hamad *et al.* [15] evaluated the residual (*i.e.* after exposure to elevated temperature) bond behaviour

146   to concrete of GFRP, BFRP, CFRP and steel bars reinforcement with different surface finishes, all

147   with embedment length of 10 times the diameter of the rebars (10 mm rebars). The pull-out

148   specimens were first exposed to elevated temperature (up to 325 ℃) and then tested at ambient

149   temperature up to failure. The bond strength reductions for specimens heated to 325 ℃ were 79%

150   for both the GFRP and BFRP rebars, 82% for the CFRP rebars and 27% for the steel rebars (all

151   compared to the corresponding bars' bond strength at ambient temperature). The authors reported

152   pull-out failure modes in specimens reinforced with GFRP, BFRP and CFRP bars (some of the

153   CFRP specimens also exhibited concrete "cone" failures), while failure in steel reinforced

154   specimens occurred due to exceeding the concrete's splitting tensile strength. Based on the

155   experimental data, Hamad *et al.* [15] also proposed temperature-dependent analytical laws to fit the

156   ascending branch of the bond stress *vs.* slip curves of the three types of rebars tested. The parameters

157   defining the analytical bond stress *vs.* slip relations were obtained from a simplistic curve fitting

158   procedure, which considered a uniform stress distribution along the embedment length of the rebars,

159   which is a very rough assumption since such distribution is well-known to be not uniform [16].

160   The literature review presented above shows that the number of existing studies about the reduction

161   with temperature of the bond properties of GFRP rebars to concrete is still very limited; therefore,

162   additional and more comprehensive investigations are required to fully understand the degradation

163   mechanisms that take place at the GFRP-concrete interface at high temperature – this knowledge

164   would contribute to improve the understanding of the structural behaviour of GFRP-RC elements

165   when subjected to fire or elevated service temperature, which, as already mentioned, is highly

166   dependent on the GFRP-concrete bond performance. Moreover, additional experimental studies are

167 also needed to further evaluate the temperature dependence of a set of parameters (for example,

168 surface finishing, diameter, geometry and embedment length in concrete), expected to affect the

169 bond properties of the rebars at elevated temperature. Finally, and unlike for steel rebars, no standard

170 bond *vs.* slip models are currently available for FRP rebars; this can be explained by the complexity

171 of modelling the FRP-concrete interaction, the non-standardized geometry and manufacturing

172 process of these bars (involving a wide variety of surface finishes and properties), as well as the

173 limited number of experimental data available, as highlighted above. So far, few bond *vs.* slip

174 models have been proposed (*e.g.* [17]), and most of them apply only for ambient temperature

175 conditions. According to the best of the authors' knowledge, apart from the study of Hamad *et al.*

176 [15], where temperature-dependent analytical laws were proposed only for the ascending branch of

177 the bond stress *vs.* slip response (and specifically for the residual behaviour), there is still no bond

178 stress *vs.* slip relations for the interaction between FRP rebars and concrete at elevated temperatures.

179 For these reasons, a perfect bond between FRP rebars and concrete is often assumed in the analytical

180 and numerical models of FRP-RC structures (*e.g.* [18–20]), leading to unrealistic and inaccurate

181 predictions of their structural performance [17]; therefore, in order to enable more accurate

182 simulations of the mechanical response of FRP-RC structural members, temperature-dependent

183 bond stress *vs.* slip local laws need to be defined.

184 **3 EXPERIMENTAL PROGRAMME**

185 *3.1 Test programme*

186 The experimental campaign presented herein comprised pull-out tests on sand coated GFRP rebars,

187 embedded in concrete cylinders, at the following six temperatures: 20 ℃, 40 ℃, 60 ℃, 80 ℃,

188 100 ℃ and 140 ℃. Two series of pull-out tests were carried out, corresponding to two different

189 embedment lengths (L_b) of the GFRP rebars into concrete: 5 and 9 times the diameter (d_b=10 mm)

190 of the rebars – 50 mm and 90 mm, respectively ($5d_b$ and $9d_b$ series). The embedment length adopted

191 in $5d_b$ series corresponds to that recommended in most test standards (*e.g.* ASTM D7913 [21] and

192 ACI 440.3R-12 [22]), whereas specimens from $9d_b$ series were produced to evaluate the influence

193 of using a longer embedment length on the GFRP-concrete bond at elevated temperature.

3.2 Description of the GFRP rebars and tensile tests at elevated temperature

The GFRP rebars used in this study were supplied by *Owens Corning* (model *Aslan 100 –* commercial diameter of 10 mm[1]); these bars are manufactured through a pultrusion process using ECR glass fibres and vinylester resin, presenting a slight surface undulation created by external helical wound fibres along with a sand coating (*cf.* Figure 1) – both the sand and the helical fibres are applied after pultrusion, but prior to thermoset of the polymeric resin [23]. The inorganic content in mass determined from burn-off tests (carried out according to [24]) is 75%.
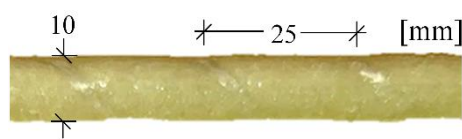
Figure 1: Sand coated GFRP rebar.

Dynamic mechanical analyses (DMA) were performed (as defined in [25]) from ambient temperature up to 250 ºC, at a heating rate of 1 ºC/min and an oscillatory frequency of 1 Hz. The results, plotted in Figure 2, allowed setting a reference T_g of 98 ºC, based on the onset of the storage modulus curve. The T_gs obtained from the peak of the loss modulus curve and the peak of the tangent delta (Tan δ) curve were 110 ºC and 121 ºC, respectively.
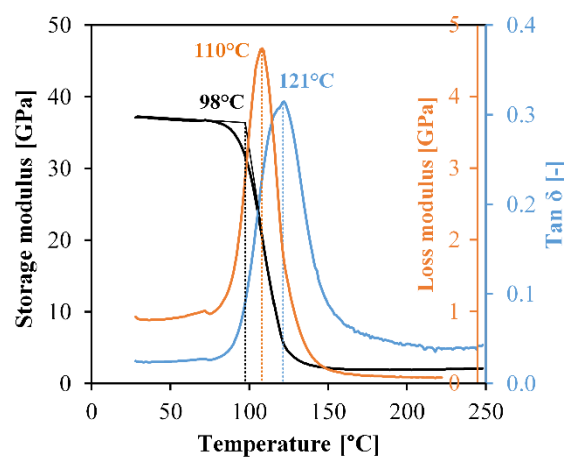
Figure 2: DMA results (storage modulus, loss modulus and tangent delta curves as a function of temperature).

---

[1] This value (10 mm) relates to the core diameter; the effective diameter of the rebar (core and surface coating) is approximately 11 mm.

206   Tensile tests were performed on the sand coated GFRP rebars according to [26] and using the test

207   setup illustrated in Figure 3. The following temperatures were tested: 20 °C (ambient

208   temperature), 50 °C, 100 °C, 150 °C, 200 °C, 250 °C and 300 °C. The rebars' temperature during

209   the tensile tests was measured in a dummy specimen, which was also placed inside the thermal

210   chamber, alongside the tested rebar; specifications of the chamber used are described in the next

211   section. The rebars were first heated up to the target temperature at an average heating rate of

212   10.7 °C/min (temperature measured in the dummy specimen) and then loaded until failure, under

213   displacement control, at an average rate of 6 mm/min. The axial deformation of the rebars was

214   measured using a video extensometer (details presented in the section) that allowed determining

215   the elastic modulus at each test temperature.
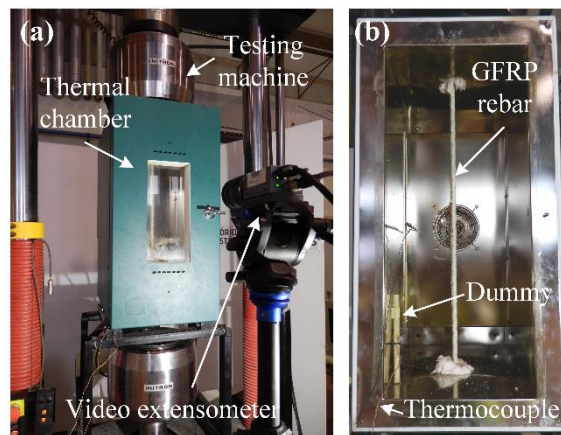
Figure 3: Setup of tensile tests: (a) general view and equipment (thermal chamber, testing machine and video extensometer); (b) tested GFRP rebar and dummy rebar inside the thermal chamber.

216   Table 1 and Figure 4 show the results obtained in terms of tensile strength and elastic modulus

217   for the different test temperatures. The tensile strength presented a significant reduction up to

218   150 °C, with strength at that temperature decreasing 40% compared to that at ambient

219   temperature. From 150 °C to 300 °C, the strength reduction was much less significant, with a

220   reduction of 43% at 300 °C. These reductions are mostly related to the degradation of the

221   polymeric matrix, as the ability to redistribute the applied load among the glass fibres is reduced,

222   promoting premature tensile ruptures. The elastic modulus was substantially less affected when

223   compared to the tensile strength, with reductions of 9% and 13% at 100 °C and 300 °C,

224   respectively. It should be noted that the steepest decrease of the tensile properties occurs roughly

225   between 50 ℃ and 100 ℃, owing to the glass transition process undergone by the polymeric

226   matrix, when the temperature approaches the T_g (set at 98 ℃, as mentioned).

227   Table 1: Tensile test results (average ± standard deviation).

Temperature [ºC]	Tensile strength [MPa]	Normalized tensile strength reduction [-]	Elastic modulus [GPa]	Normalized elastic modulus reduction [-]
20 ± 2	1045.1 ± 8.4 (0.8%)	-	48.2 ± 0.8 (1.7%)	-
50 ± 2	927.5 ± 8.0 (0.9%)	11%	47.6 ± 0.1 (0.2%)	1%
100 ± 2	682.4 ± 14.6 (2.1%)	35%	44.1 ± 1.2 (2.7%)	9%
150 ± 2	623.2 ± 30.6 (4.9%)	40%	45.9 ± 1.3 (2.8%)	5%
200 ± 2	603.7 ± 15.1 (2.5%)	42%	45.3 ± 2.2 (4.9%)	6%
250 ± 2	619.3 ± 11.2 (1.8%)	41%	43.7 ± 3.6 (8.2%)	9%
300 ± 2	598.2 ± 23.5 (3.9%)	43%	41.8 ± 4.1 (9.8%)	13%
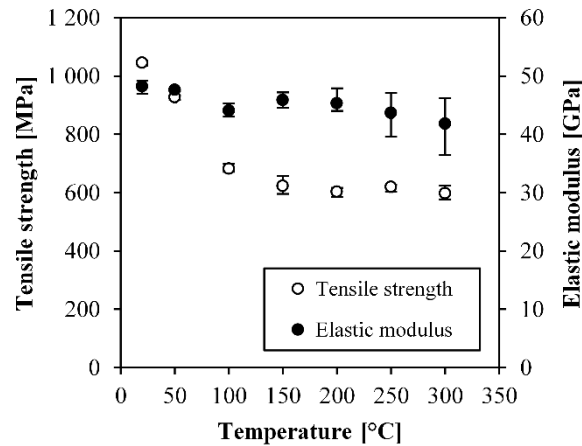
Figure 4: Tensile properties of GFRP rebars as a function of temperature (average ± standard deviation values).

228   **3.3 Description of pull-out specimens, instrumentation and test procedure**

229   Concrete class C25/30 with cement type CEM II/A-L 42.5R and limestone aggregates was used

230   to produce the specimens for the pull-out tests. The concrete's tensile and compressive properties

231   were determined at the age of the pull-out tests (111 days). During that period, the test specimens,

232   as well as the cylinders and cubes used to characterize the concrete's properties, were cured in

233   the laboratory facilities at ambient temperature and relative humidity (indoor, but not controlled).

234   The compressive and splitting tensile strength tests were performed according to standard

235 procedures ([27] and [28], respectively), providing the following average values: cube

236 compressive strength of 43.3 MPa and splitting tensile strength of 3.1 MPa.

237 The test specimens consisted of concrete cylinders (height and diameter of 150 mm) with a single

238 GFRP rebar (total length of 745 mm) embedded vertically ($5d_b$ or $9d_b$) along the central axis of

239 the cylinder.

240 The unbonded length of the rebars was set using a bond breaker made of a PVC tube (outer

241 diameter of 16 mm, 1.3 mm thick), as shown in Figure 5. At the free end, the rebars were slightly

242 protruded from the concrete cylinder, thus allowing to read the slip between that end of the rebars

243 and the top surface of the concrete (using a video extensometer, as explained below). The loaded

244 end of the rebars was protected using stainless steel tubes (outer diameter of 22 mm, 0.7 mm

245 thick) to prevent premature tensile failure at the grip of the testing machine (*cf.,* Figure 6).
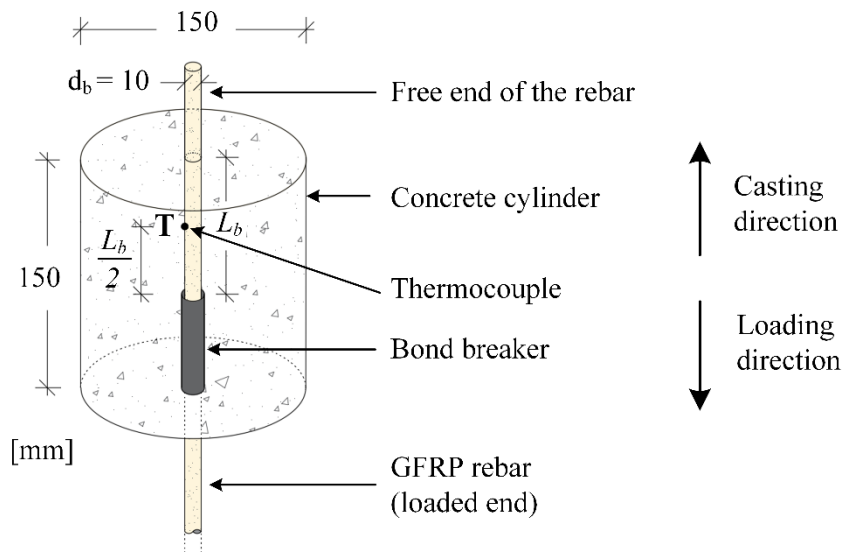
Figure 5: Pull-out test specimen geometry and thermocouples placement.

246 The setup used in the pull-out tests is illustrated in Figure 6. The specimens were positioned in a

247 frame composed by two metal plates, connected with steel rods, which acted as a reaction device.

248 The frame was installed inside a *Tinius Olsen* thermal chamber (*cf.* Figure 6b) and was coupled

249 to an *Instron* universal testing machine with load capacity of 250 kN (*cf.* Figure 6c). The

250 specimens' temperature was measured with type K thermocouples (0.25 mm of conductor

251 diameter), positioned at mid-height of the embedment length (*cf.* Figure 5). An additional

252 thermocouple was used to control the temperature of the air inside the thermal chamber. The slip

253 of the rebars was measured at both free and loaded ends using a video extensometer (*cf.* Figure

254 6b); this equipment consists of a high definition video camera (*Sony*, model *XCG 5005E*, with

255 *Fujinon* lens, model *Fujifilm HF50SA-1*) placed on a tripod. As illustrated in Figure 6a, target

256 dots were marked on the GFRP rebar (on both free and loaded ends) and on angle brackets (fixed

257 to the concrete's surface and to the bottom steel plate, respectively), allowing to measure the

258 relative displacement (*i.e.*, the slip) between the rebar and the concrete.
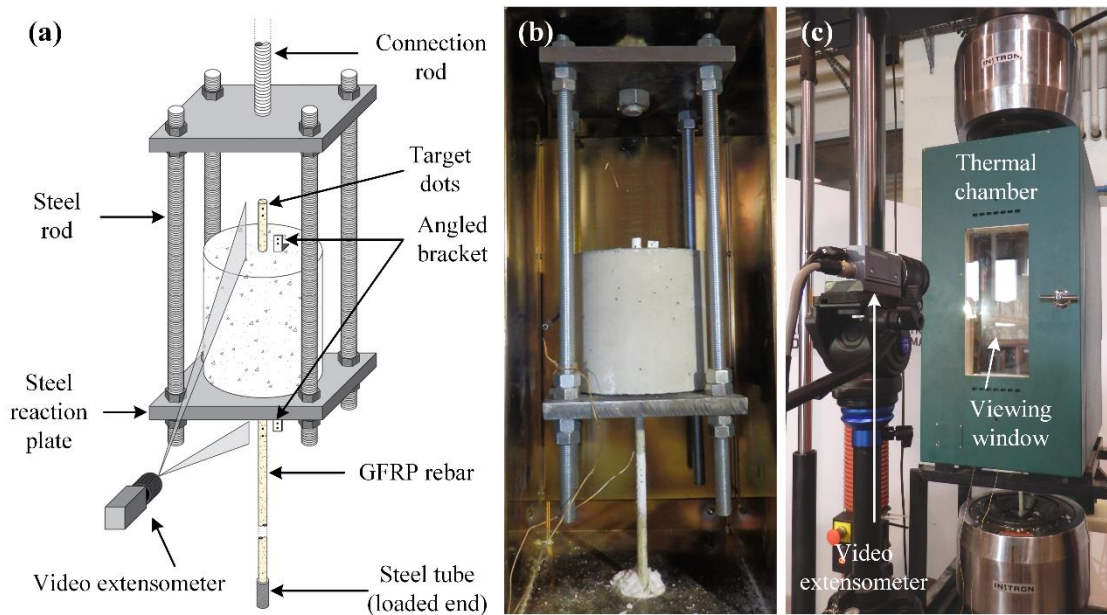
Figure 6: a) Setup of pull-out tests; (b) general view of the specimen in the thermal chamber;
(b) external view of the thermal chamber and video extensometer.

259 The experimental procedure was divided in two stages. In the first stage, the specimens were

260 heated up to the predefined (target) temperature at an average heating rate of the air inside the

261 thermal chamber of 10 °C/min (0.9 °C/min at the GFRP-concrete interface). In order to minimize

262 the specimen's heating time, the initial temperature of the thermal chamber was set 10 °C above

263 the specimen's target temperature. Once the temperature at the GFRP-concrete interface (from

264 now on referred to as "specimen temperature") approached the target temperature (*i.e.*, 2 °C

265 lower), the temperature of the thermal chamber was reduced (to the target value), guaranteeing a

266 constant temperature in the specimen during the second stage of the tests (*i.e.,* the loading stage,

267 as described below). This procedure is exemplified in Figure 7, which shows, for two different

268 target temperatures (80 ℃ and 140 ℃), the temperature-time curves of both the specimens and

269 the air inside the thermal chamber. It is worth mentioning that during the first stage of the test

270 procedure the lower grip of the testing machine was kept open, thus avoiding any axial restriction

271 due to thermal expansion of the specimens.

272 The second stage, during which the specimens' temperature was kept constant at the predefined

273 target value, consisted of loading the specimens (*i.e.*, pulling the GFRP rebars) until failure, under

274 displacement control, at an approximate speed of 1 mm/min (test speed defined according to the

275 limits set in ASTM D7913 [21]). During this stage, the applied load, the cross-head displacement

276 of the test machine and the position of the target dots were monitored. The tests were carried out

277 until the target dots were no longer traceable by the video extensometer (due to the limited height

278 of the furnace's viewing window). For each temperature and embedment length, at least three

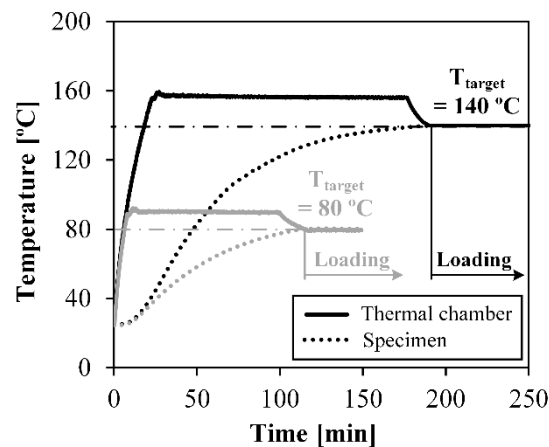279 replicate specimens were tested.

Figure 7: Temperature-time curves of the specimens (measured at concrete-GFRP interface) and of the air inside the thermal chamber, for different target temperatures (80 ℃ and 140 ℃).

4 EXPERIMENTAL RESULTS AND DISCUSSION

4.1. Bond stress *vs*. slip curves

282 Figure 8 and Figure 9 present for each target temperature and embedment length ($5d_b$ and $9d_b$

283 series) the average bond stress *vs.* slip curves, with the slip measured at the free and loaded ends

284 of the rebars, respectively. To simplify the analysis described in the present section, the curves

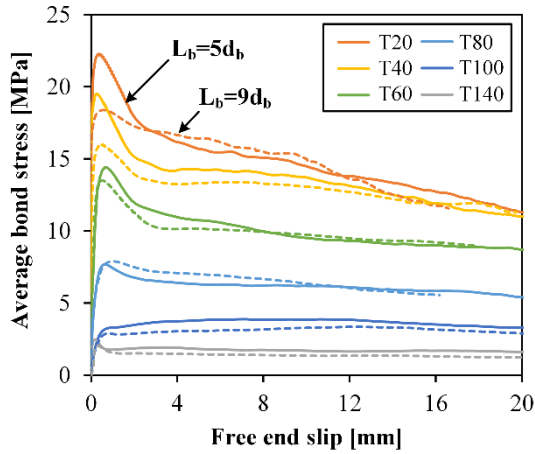285 are only plotted up to slips of 20 mm.

Figure 8: Average bond stress *vs.* slip curves (slip measured at the free end) for all tested temperatures (*5d_b* series – continuous line; *9d_b* series – dashed line).
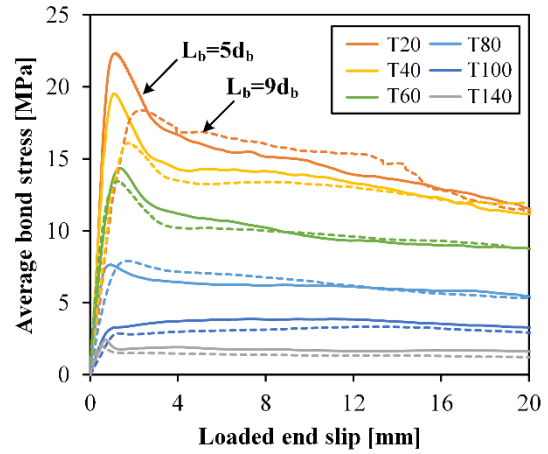
Figure 9: Average bond stress *vs.* slip curves (slip measured at the loaded end) for all tested temperatures (*5d_b* series – continuous line; *9d_b* series – dashed line).

286 Regardless of the embedment length, the curves present an approximately linear behaviour until

287 the maximum stress was attained; the slope of these ascending branches (*i.e.* the bond stiffness)

288 was progressively reduced as the test temperature increased – this stiffness reduction is clearly

289 noticed in Figure 9. After the average bond strength was attained, a stress drop occurred (with

290 exception of the specimens tested at 100 ºC, where a stress peak did not occur and consequently

291 no such drop exists); this drop was then followed by a progressive stress reduction, with the curves

292 exhibiting almost a plateau for higher slips. This final stage of the curves extended up to the end

293 of the tests, which were interrupted before the complete pull-out of the rebars (due to the loss of

294 the target dots, as mentioned in section 3.3). The specimens tested at 100 ºC presented a different

295 post-peak behaviour compared to the remaining ones: after the average bond strength was attained

296 (which occurred for considerably higher slip values), the stress values presented a progressive

297 reduction - this behaviour may be related to the fact that this temperature virtually matches the T_g

298 of the rebars (98 ºC), for which the viscoelasticity of the material is known to be maximum.

299 As shown in Figure 8 and Figure 9, the curves obtained at the free and loaded ends of the

300 specimens presented a similar overall behaviour. However, the following differences should be

301 noted: while the slip at the loaded end of the rebars increased from the beginning of the loading

302 stage (*cf.* Figure 9), the same did not occur at the free end - for specimens tested at 20 ºC and

303   40 ºC, as expected, the initial branch of the curves is approximately vertical (*i.e.,* the slip at the

304   free end is negligible); this indicates the bond length was only partially mobilized for relatively

305   high stress values, *i.e.* up to approximately the average bond strength (*cf.* Figure 8); the moment

306   when the free end slip presents a significant increase should be related to the loss of adhesion

307   between the sand coating and the core of the rebar (further discussion is provided in section 4.2).

308   However, for specimens tested at temperatures above 40 ºC, the slip at the free end starts as soon

309   as loading begins, which indicates that even relatively low temperatures (including below the

310   rebar's T_g) have a non-negligible effect on the degradation of the rebar-concrete bond, particularly

311   on the sand coating-rebar's core interface.

312   The plateau branch of the curves after the stress peak should have been caused by the progressive

313   penetration of the free end length of the rebars into the concrete cylinder (note that this stems

314   from the standard test setup adopted). When in contact with the concrete's surface, this

315   undamaged (mechanically) portion of the rebars may have provided an increase in the

316   GFRP-concrete friction, compared to the one afforded by the damaged (and initially embedded)

317   length of the rebars, thus providing an additional contribution to the overall resistance against

318   slip.

319   Figure 8 and Figure 9 also show that: (i) for a certain temperature, as expected, the specimens

320   with longer embedment length ($9d_b$ series) presented lower average bond stresses; and (ii) the

321   bond strength was progressively reduced with temperature (*cf.* Table 1 and Table 2). The effect

322   of elevated temperature was also noticeable in the bond stiffness reduction (corresponding to the

323   slope of the initial linear branch); this result was also expected, since for elevated temperatures

324   the stiffness and strength of the constituent materials and especially of the GFRP-concrete

325   interface are reduced. Figure 10 presents for each target temperature and embedment length the

326   load *vs.* free end slip curves; this figure allows confirming that specimens with longer embedment

327   length ($9d_b$ series) attained higher loads and, for those specimens, slip starts to increase for higher

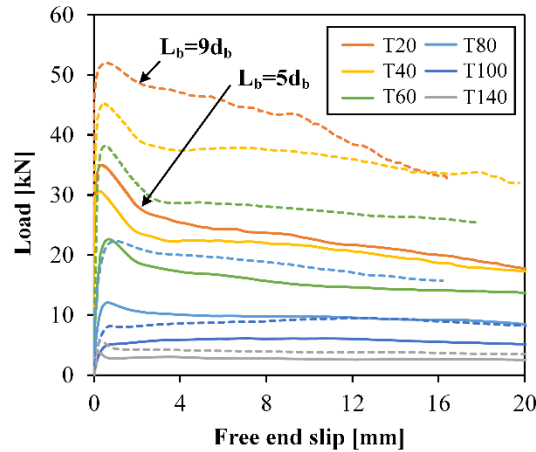328   load values comparing to the $5d_b$ series.

Figure 10: Load *vs.* slip curves (slip measured at the free end) for all tested temperatures (*5d_b* series – continuous line; *9d_b* series – dashed line).

4.2. Failure modes and post pull-out observations

330   For all test temperatures, failure of specimens from *5d_b* series occurred due to pull-out of the

331   GFRP rebars, *i.e.* slippage of the rebars along the embedment length in the concrete cylinder. The

332   experimental results (described in the previous section) and the visual observations of the

333   specimens throughout the tests (*e.g.,* Figure 11) confirmed the occurrence of this expected failure

334   mode.

335   Regarding the specimens from *9d_b* series, in general pull-out of the rebars also occurred, with the

336   exception of some specimens tested at ambient temperature, which presented splitting of the

337   concrete. In order to avoid this type of failure (and to obtain the desired pull-out failure),

338   additional specimens were confined using four stainless steel clamps (28 mm wide) evenly

339   distributed along the height of the cylinder. The tests on these specimens (carried out at ambient

340   temperature) showed that despite the confinement provided to the concrete (which successfully

341   avoided splitting failures), the bond stress *vs.* slip response was not affected, presenting a similar

342   behaviour (*i.e.*, identical stiffness of the ascending branch and maximum average bond stress) to

343   that obtained in unconfined specimens (*cf.* section 4.1). Indeed, the maximum value of the average

344   bond stress obtained in the confined and unconfined specimens was very similar: 19.4 and
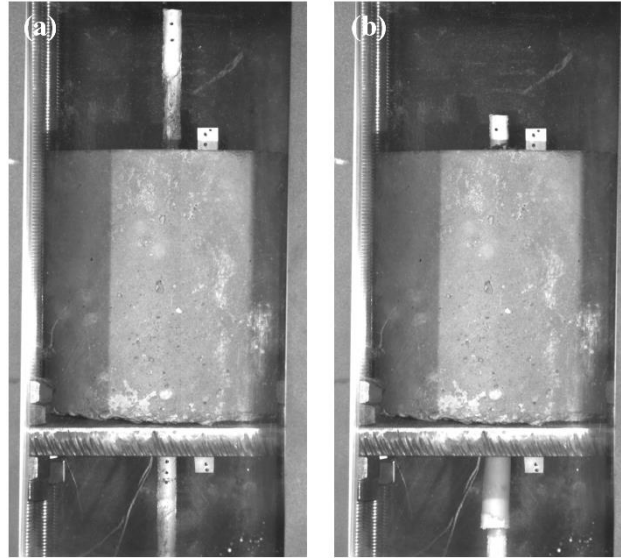
345   19.2 MPa, respectively.

Figure 11: Pull-out of the rebars from the concrete cylinders: representative specimen at (a) the beginning and (b) end of the tests.

346　After the tests, all concrete cylinders were sawn cut into two pieces to confirm the failure modes

347　and evaluate the damage underwent by the materials and at the rebars-concrete interface. As shown

348　in Figure 12a, in specimens tested at elevated temperatures the external layer of the GFRP rebars

349　was significantly abraded, with exposure of the longitudinal and wound fibres; in particular, the

350　wound fibres were ripped and the superficial sand-coated layer was peeled; residues of crushed

351　resin, some broken wound fibres and most of the sand particles were attached to the concrete (along

352　the embedment length of the rebar); no damage on the core of the rebars was observed. In the

353　specimens tested at ambient temperature (Figure 12b), the abrasion introduced to the rebar was

354　more severe: the superficial sand-coated layer and the wound fibres were completely removed, the

355　core of the rebar was exposed and some longitudinal fibres were broken and stripped from the core.

356　The visual inspections of the pull-out specimens after the tests demonstrated that the bond behaviour

357　of the sand-coated GFRP rebars to concrete, at both ambient and elevated temperatures, was

358　influenced by the adhesion (and friction) between the surface finishing (sand coating and wound

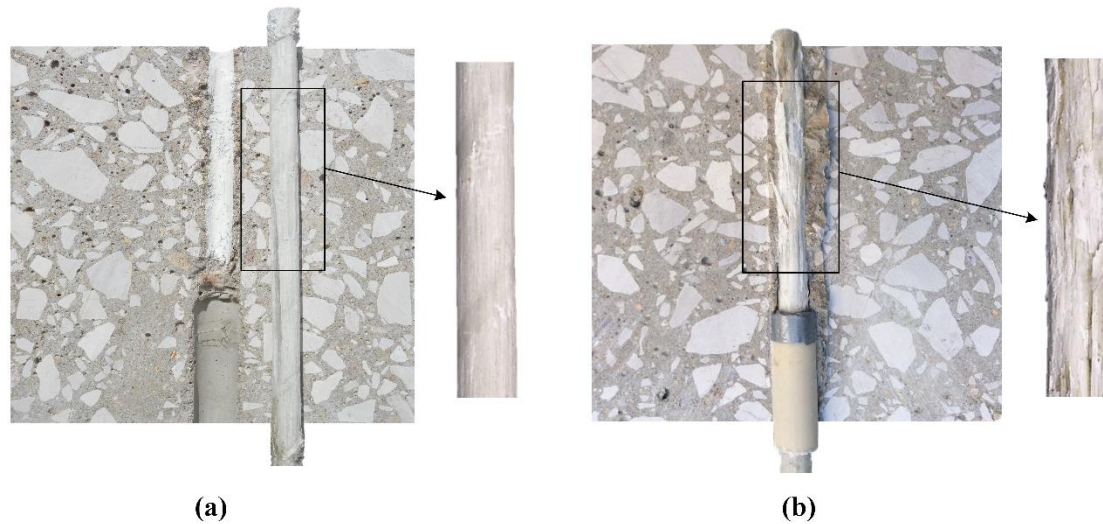359　fibres) and the rebar's core.

(a)   **(b)**

Figure 12: Surface of the GFRP rebar after testing at (a) elevated temperature and (b) ambient temperature.

4.3. Bond strength and stiffness

360

361 Figure 13 presents the variation with temperature of the following parameters (normalized

362 average values): (i) the average bond strength; (ii) the bond stiffness (corresponding to the slope

363 between 25 and 50% of the maximum value of the bond stress *vs.* loaded end slip curves); (iii)

364 the tensile strength, (iv) the elastic modulus, and (v) the storage modulus curve (obtained from

365 DMA tests) of the rebars. Table 2 and Table 3 summarize the results obtained for series $5d_b$ and

366 $9d_b$, respectively.

367 The results depicted in Figure 13 show that the bond strength was significantly reduced with

368 temperature, even for values well below the T_g of the GFRP rebars. For temperatures as low as

369 60 ºC (that can be attained in outdoor applications), bond strength reductions were at least 29%,

370 while for 100 ºC and 140 ºC, the reductions were around 80% and 90%, respectively. Moreover,

371 the results depicted in Figure 13 highlight that: (i) the bond strength exhibited a similar reduction

372 with temperature for the two test series (*i.e.*, for the two different embedment lengths); (ii) the

373 reduction of the GFRP-concrete bond strength (and stiffness) occurred for lower temperatures

374 than the mechanical degradation at the material level (as measured in the tensile tests and in the

375 DMA tests).

18

376   Table 2 and Table 3 show that for temperatures up to 60 ºC for $5d_b$ series and 80 ºC for $9d_b$ series,

377   the ratio between the maximum tensile stress developed in the GFRP rebars during the pull-out

378   tests and the tensile strength of the rebars at ambient temperature is higher than 25%; in most

379   design guidelines, this value is defined as the maximum stress level that can be developed in the

380   GFRP rebars for serviceability limit state. Regarding the stiffness of the GFRP-concrete interface,

381   the results obtained also show that it was significantly affected by temperature: (i) at 60 ºC, the

382   bond stiffness reduction was at least 44%, progressing to 80% at 100 ºC; and (ii) the steepest

383   reduction occurred (below the T_g) in specimens with a shorter embedment length. It is still worth

384   noting that in both series the bond stiffness presented an increase when the tested temperature

385   raised from 100 ºC to 140 ºC, especially for $9d_b$ series – this result (unexpected *a priori*) may be

386   partially explained by the fact that for such temperature variation the radial expansion of the rebar

387   was possibly more significant than the thermal degradation of the materials; therefore, it may

388   have increased the friction between the rebar's core and the superficial surface finishing and,

389   consequently, the bond stiffness. Additional investigations are needed to confirm this
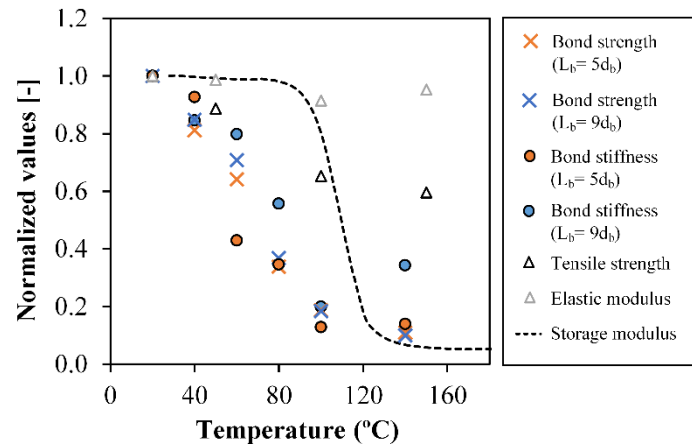
390   phenomenon.

Figure 13: Normalized values of bond strength and stiffness, tensile strength, elastic modulus
and storage modulus of the GFRP rebars as a function of temperature.

391

392

393

Table 2: Test results obtained from specimens with embedment length of 5d_b (average ± standard deviation).

Embedment length to concrete = 5d_b							
Temperature [ºC]	Maximum load [kN]	Average bond strength [MPa]	Normalized bond strength reduction [-]	Ratio maximum axial stress/tensile strength at elevated temperature	Ratio maximum axial stress/tensile strength at ambient temperature	Bond stiffness (loaded end) [MPa/mm]	Normalized bond stiffness reduction [-]
20 ± 2	36.3 ± 3.2	23.1 ± 2.0	-	49%	49%	34.9 ± 3.3	-
40 ± 2	29.4 ± 2.0	18.7 ± 1.3	19%	43%	39%	32.4 ± 10.6	7%
60 ± 2	23.3 ± 1.3	14.8 ± 0.8	36%	37%	31%	15.0 ± 5.7	57%
80 ± 2	13.8 ± 3.1	8.8 ± 2.0	66%	25%	18%	12.1 ± 4.7	65%
100 ± 2	6.8 ± 1.3	4.3 ± 0.8	81%	14%	9%	4.5 ± 1.3	87%
140 ± 2	4.0 ± 0.3	2.5 ± 0.2	89%	9%	5%	4.9 ± 1.2	86%

Table 3: Test results obtained from specimens with embedment length of 9d_b (average ± standard deviation).

Embedment length to concrete = 9d_b							
Temperature [ºC]	Maximum load [kN]	Average bond strength [MPa]	Normalized bond strength reduction [-]	Ratio maximum axial stress/tensile strength at elevated temperature	Ratio maximum axial stress/tensile strength at ambient temperature	Bond stiffness (loaded end) [MPa/mm]	Normalized bond stiffness reduction [-]
20 ± 2	54.6 ± 3.1	19.3 ± 1.1	-	73%	73%	14.7 ± 1.8	-
40 ± 2	46.5 ± 2.0	16.4 ± 0.7	15%	67%	62%	12.5 ± 1.0	15%
60 ± 2	38.8 ± 5.5	13.7 ± 2.0	29%	62%	52%	11.8 ± 1.2	20%
80 ± 2	20.1 ± 3.2	7.1 ± 1.1	63%	36%	27%	8.2 ± 0.1	44%
100 ± 2	10.1 ± 2.7	3.6 ± 1.0	82%	21%	14%	3.0 ± 0.9	80%
140 ± 2	5.5 ± 0.4	1.9 ± 0.2	90%	12%	7%	5.1 ± 1.8	66%

Figure 14 presents a comparison of the normalized bond strength obtained in this study with the test data reported by Katz *et al.* [7] and McIntyre *et al.* [12]; these studies, reviewed in section 2, deal with pull-out tests in GFRP rebars with similar surface finishing (sand coating) and the same test procedures (the loading stage took place while the specimens were at a constant (elevated) target temperature). It should be noted that: (i) the GFRP rebars used in these two studies were produced by different manufacturers and had different nominal diameters; (ii) the embedment lengths to concrete were similar (5d_b and 4d_b for the first and second studies, respectively); (iii) in the study of McIntyre *et al.*, the predominant failure mode was by splitting of the concrete; (iv) in the present study and in the study of Katz *et al.* pull-out failure modes occurred at all tested temperatures.

408   The results plotted in Figure 14 show that the bond strength reduction with temperature obtained

409   in the various studies is qualitatively similar, exhibiting the same general trend. However, in the

410   present study, for temperatures ranging from 60 ºC to 140 ºC the reduction of bond strength was

411   higher when compared to the other two studies. No evident relation between the bond strength

412   decay and the T_gs of the rebars was found that could justify such difference. A possible

413   explanation for this result may be related to different surface properties of the rebars, namely the

414   adhesion between the superficial finishing and the core - as discussed in section 4.2, the behaviour

415   of this interface seems to play a significant role on the bond performance of this type of FRP

416   reinforcement. In the present study the damage observed in the rebars after testing (*cf.* section

417   4.2) was similar to that reported by the above-mentioned authors.
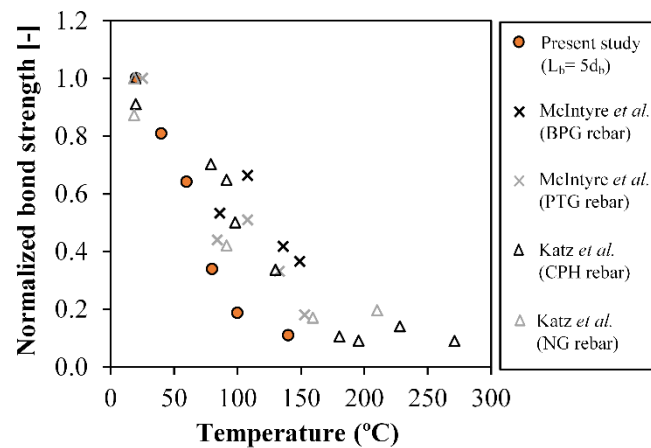
(BPG: Double helical fibre wrap with a fine sand coating, T_g=86ºC (DMA). PTG: Coarse sand coating, T_g=84ºC (DMA). CPH: Helical fibre wrap and sand coating, T_g=122ºC (test method not specified). NG: Helical fibre wrap and sand coating with surface deformations, T_g=60ºC (test method not specified))

Figure 14: Comparison of the bond strength: results obtained in the present study and those from
McIntyre *et al.* [12] and Katz *et al.* [7].

418   **5   ANALYTICAL STUDY**

419   **5.1. Bond stress vs. slip curves**

420   The bond behaviour between reinforcing bars and concrete is usually described through bond

421   stress *vs.* slip models. As discussed in section 2, such models for the simulation of the influence of

422   the temperature on the GFRP-concrete bond behaviour are still not available in the literature. In the

423   present section, a numerical method, developed and detailed by Sena-Cruz and Barros in [16], is

424   used to obtain such relations for the sand-coated GFRP rebars used in this study for temperatures

425   up to 140 ℃ and an embedment length of $5d_b$.

426   The method is based on a numerical approach in which the experimental results (*i.e.*, the load *vs.*

427   slip results) are used to calibrate a set of parameters defining the analytical bond stress *vs.* slip law.

428   In addition to the geometric features of the rebars (cross section and bond length to concrete), the

429   results obtained in terms of elastic modulus as a function of temperature (described in section 4.2)

430   are also used as input to calibrate the analytical laws.

431   The computational code developed by Sena-Cruz and Barros [16] was used to solve the differential

432   Equation (1) that governs the slip of a GFRP rebar along the embedment length to the concrete,

$$\frac{d^2 s}{dx^2} = \frac{4}{d_b E_f} \tau(s) \qquad (1)$$

433   where s is the slip, x is the positioning along the embedment length, $\tau(s)$ is the bond stress for a

434   certain slip value, d_b is the diameter and E_f the elastic modulus of the rebar. The analytical

435   expression considered for the local bond stress *vs.* slip relationship was proposed by Sena-Cruz [29]

436   and is defined by the following equations,

$$\tau(s) = \begin{cases} \tau_m \left(\dfrac{s}{s_m}\right)^\alpha & if\ s \le s_m \qquad (2a) \\[3mm] \tau_m \dfrac{1}{1 + \left(\dfrac{s - s_m}{s_1}\right)^{\alpha'}} & if\ s > s_m \qquad (2b) \end{cases}$$

437   where τ_m and s_m are the bond strength and the corresponding slip, and α, α' and s_1 are the

438   parameters defining the shape of the bond stress *vs.* slip curves. Equation (2a) defines the $\tau(s)$ for

439   the pre-bond strength phase , following the model proposed by Eligehausen *et al.* [30], while

440   Equation (2b) simulates the post-peak phase (slip softening stage), following the approach of Stang

441   and Aarre [31]. It is worth highlighting that the numerical method used in the present study considers

442   a non-uniform distribution of the bond stress along the embedment length of the rebars.

443   The numerical methodology adopted herein was successfully used earlier to model the bond

444   behaviour of near-surface mounted (NSM) CFRP strips and concrete [16]. However, in the present

445   study, when using the elastic modulus of the rebars obtained from the tensile tests, the resulting

446   analytical load *vs.* slip curve (obtained for the slip at the loaded end) presented a significantly higher

447   stiffness (as defined by the slope of the initial linear branch) than that measured in the experiments.

448   This deviation, exemplified in Figure 15 for a temperature of 20 ºC, was consistent for all test

449   temperatures. However, in a similar campaign carried out by the authors in ribbed GFRP rebars,

450   these relative differences were not observed: the analytical load *vs.* slip curves reproduced quite

451   accurately the experimental data, as exemplified in Figure 17 for a temperature of 20 ºC.

452   The authors believe that the relative differences obtained for the sand coated rebars (which did not

453   occur for the ribbed rebars) is related to the deformability of its constituent materials/layers; in fact,

454   in a few specimens it was quite clear that slippage occurred mainly between the core of the rebars

455   and its superficial sand coating, as already mentioned in section 4.1. Therefore, these evidences

456   suggested that the rebars could be seen as a composite reinforcement, in which the deformability of

457   the core and that of the superficial layer of sand and resin are different. Therefore, the heterogeneity

458   of the rebars throughout its thickness was addressed (numerically) by calibrating, for each

459   temperature, an apparent elastic modulus (as a percentage of the modulus experimentally obtained).

460   This approach allowed for a significant accuracy increase regarding the stiffness of the analytical

461   load *vs.* slip curves (slip measured at the loaded end), as exemplified in Figure 16, also for a

462   temperature of 20 ºC. The temperature-dependent calibrated values (used to obtain the analytical

463   local bond stress *vs.* slip laws) of the apparent elastic modulus of the GFRP rebar are listed in Table
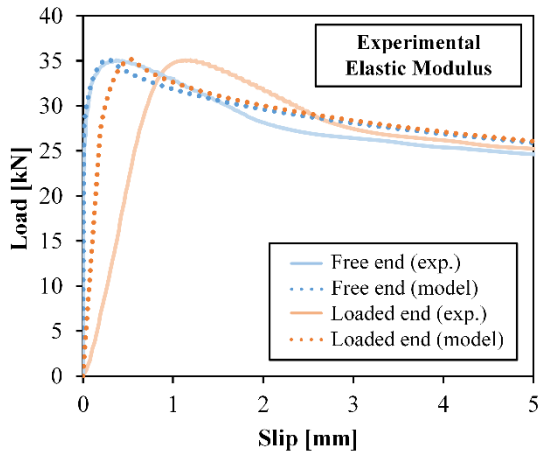
464   4.

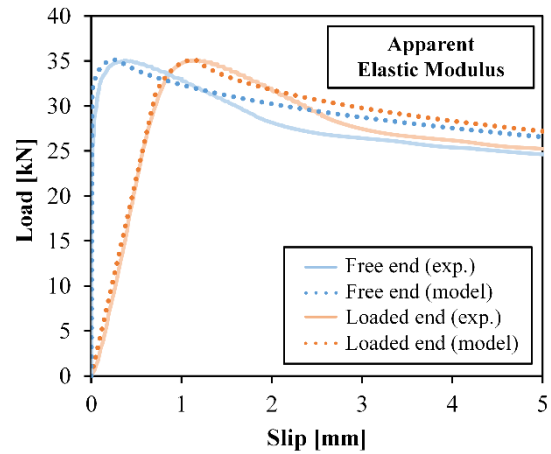Figure 15: Comparison between experimental and analytical load *vs.* slip curves at T=20 ℃: modelling using the elastic modulus obtained from tensile tests.

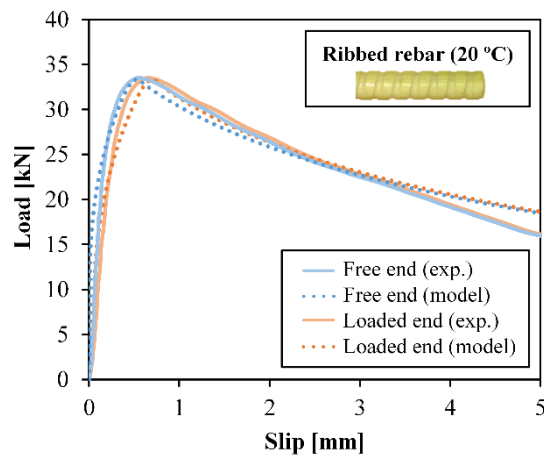Figure 16: Comparison between experimental and analytical load *vs.* slip curves at T=20 ℃: modelling using the apparent (calibrated) elastic modulus.

Figure 17: Comparison between experimental and analytical load *vs.* slip curves for a ribbed rebar tested at T = 20 ℃: modelling using the elastic modulus obtained from tensile tests.

465   The parameters defining the calibrated local bond stress *vs.* slip laws (*cf.* Figure 20) are listed in

466   Table 4; they were obtained by minimizing the relative difference (area) between the experimental

467   and analytical load *vs.* slip curves (obtained for both free and loaded ends) and by ensuring similar

468   values of maximum load and corresponding slip. The comparison between the experimental and

469   analytical curves is plotted in Figure 18 (for the slip at the free end) and in Figure 19 (for the slip

470   at the loaded end), demonstrating the overall good performance of the numerical strategy adopted

471   for deriving the bond stress *vs.* slip relationship in the context of modelling the GFRP-concrete

472   interface. This is also attested by the low values of relative difference obtained (below 7%, *cf.*

473   Table 4), indicating a very good fit of the analytical curves to the experimental data. As previously

24

mentioned (*cf.* section 4.1), the behaviour of the specimens tested at 100 °C was somehow

different from the specimens tested at the other temperatures. For this reason, a better fit of the

experimental data could have been obtained by using a different analytical expression for the local

bond law than the one chosen in this study (Equation 2b); nevertheless, the results obtained herein
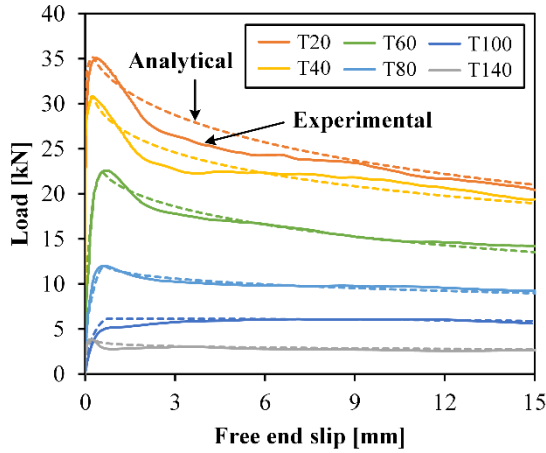
were quite satisfactory.

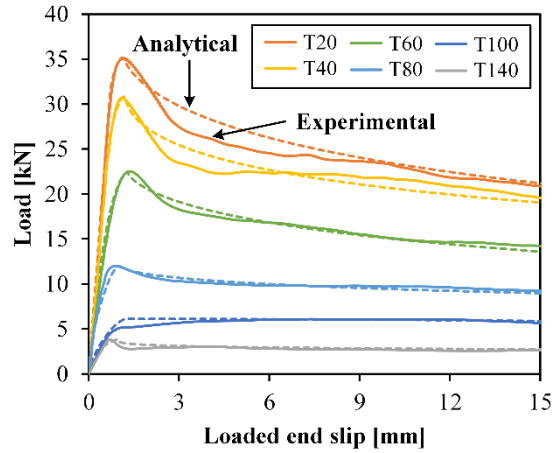Figure 18: Comparison between the experimental (continuous) and analytical (dashed) load *vs.* free end slip curves.

Figure 19: Comparison between the experimental (continuous) and analytical (dashed) load *vs.* loaded end slip curves.

Table 4: Parameters defining the calibrated local bond-stress *vs.* slip relationship.

Series	T [ºC]	Calibrated elastic modulus [GPa]	s_m [mm]	τ_m [MPa]	α [-]	α' [-]	s_1 [-]	Relative difference[1] [-]	
								Free end slip	Loaded end slip
T20_5d$_b$	20	14.5 (30% E_{exp})	0.32	23.70	0.15	0.59	20	4.2%	4.8%
T40_5d$_b$	40	12.0 (25% E_{exp})	0.35	21.80	0.25	0.44	20	3.8%	4.5%
T60_5d$_b$	60	11.7 (25% E_{exp})	0.61	15.00	0.50	0.59	24	2.1%	2.5%
T80_5d$_b$	80	11.0 (24% E_{exp})	0.69	7.90	0.45	0.45	120	2.5%	2.7%
T100_5d$_b$	100	4.4 (10% E_{exp})	0.75	3.90	0.50	2.00	70	3.9%	3.7%
T140_5d$_b$	140	2.2 (10% E_{exp})	0.40	2.91	0.50	0.20	110	6.4%	6.6%

[1] Relative percentage difference, in absolute value, between the areas below the experimental and analytical load *vs.* slip curves (slip measurements at the free and loaded ends of the rebar).

The calibrated GFRP-concrete bond constitutive laws obtained for each of the tested temperatures

are plotted in Figure 20. These curves prompt the following main remarks: (i) the maximum bond

482   stress and stiffness are progressively reduced as temperature increases; (ii) for all temperatures,

483   at relatively high slip values a significant bond stress is retained; (iii) up to 100 ℃, the slip

484   corresponding to the bond strength (s_m) increases with temperature, while from 100 ℃ to 140 ℃,

485   such slip is significantly reduced (*cf.* Table 4). This non-monotonic variation of the slip

486   corresponding to the maximum bond stress should be related to the thermo-physical changes

487   undergone by the polymer during the glass transition process, whose viscosity presents a

488   maximum during glass transition (the peak of the loss modulus curve occurs at 110 ℃),
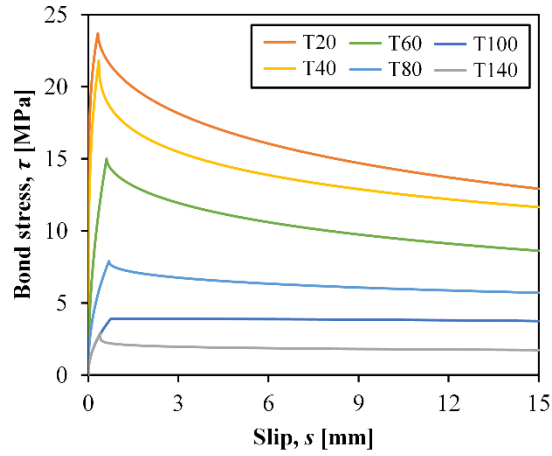
489   decreasing for lower and higher temperatures.

Figure 20: Calibrated local bond stress *vs.* slip relationship for different temperatures.

490   **5.2. Bond strength degradation models**

491   In this subsection, the ability of the empirical models proposed by Gibson *et al.* [32] and Correia *et al.*

492   [33] in simulating the variation of the bond strength with temperature was assessed. These relaxation

493   models involve curve fitting procedures to the experimental results and have been successfully used

494   to simulate the mechanical properties of FRP materials at elevated temperatures [33].

495   According to Gibson *et al.* [32], the variation of a generic mechanical property (*P*) with

496   temperature (*T*) can be defined by the following equation,

$$P(T) = P_u - \frac{P_u - P_r}{2} \times (1 + \tanh[k'(T - T_{g,mech})]) \tag{3}$$

497   where P_u is the value of the property at ambient temperature and P_r is the value of the property

498   after the glass transition (but before decomposition). The parameters k' and $T_{g,mech}$ are obtained

499   by fitting the theoretical curve to the experimental data.

500   Correia *et al.* [33] proposed the following model, which is based on the Gompertz statistical

501   distribution, where the parameters B and C are fitted to the experimental data:

$$P(T) = P_r + (P_u - P_r) \times (1 - e^{Be^{C \times T}}) \tag{4}$$

502   Since the bond strength obtained for both embedment lengths presented a similar reduction with

503   temperature, the equations described above were simultaneously fit to the experimental data of

504   both lengths using a standard procedure that minimizes the mean square errors.

505   Figure 21 plots the fitting curves for both models, together with the normalized experimental

506   values of the bond strength. Table 5 lists the values of the parameters obtained for the two models

507   and the respective absolute mean percentage error (AMPE). It can be seen that both models

508   present a very good agreement with the experimental results (slightly better for the model of

509   Gibson *et al.*), *i.e.,* they are able to provide accurate estimates of the GFRP-concrete bond strength

510   reduction with temperature.
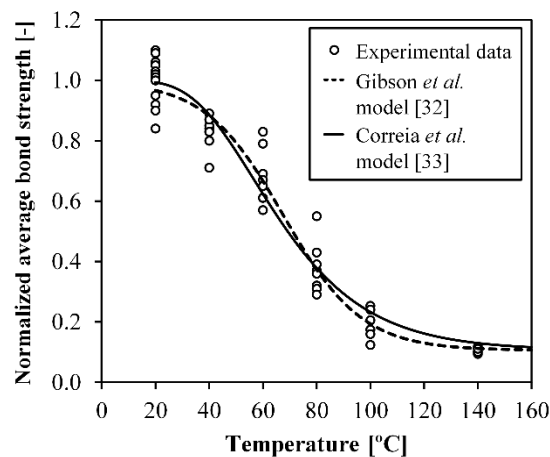
511

512   Figure 21: Normalized average bond strength (compared to ambient temperature) vs.
513   temperature: experimental results and modelling curves.

514

515

Table 5: Simulation of the bond strength degradation with temperature – defining parameters and absolute mean percentage error (AMPE).

Model	Parameter	
Gibson *et al.* [32]	k' [-]	0.0342
	$T_{g,mech}$ [ºC]	67.59
	AMPE [%]	10.8
Correia *et al.* [33]	B [-]	-11.68
	C [-]	-0.0433
	AMPE (%)	14.0
$P_u = 1.00$		$P_r = 0.11$

6 CONCLUSIONS

This paper presented experimental and analytical investigations about the bond behaviour between GFRP rebars (sand coated with external helically wound fibres) and concrete from ambient temperature up to 140 ºC. From the results obtained, the following main conclusions can be drawn:

1. The results confirmed the degradation of the tensile properties of GFRP rebars at elevated temperature: the tensile strength was considerably reduced when the T_g (98 ºC) was reached, with retentions of 60% and 57% at 150 ºC and 300 ºC, respectively; the elastic modulus was significantly less affected, presenting retentions of 95% and 87% for those temperatures.

2. As expected, the strength and stiffness of the GFRP-concrete interface were significantly affected with increasing temperatures. The average bond strength was severely reduced for temperatures well below the T_g of the GFRP rebars, presenting reductions of 29% and 89% at, respectively, 60 ºC and 140 ºC, compared to the average bond strength at ambient temperature. The bond stiffness (measured at the loaded end) experienced reductions of 44% and 80% at 60 ºC and 100 ºC, respectively, comparing to the stiffness at ambient temperature. For the materials, test setup and procedure, and range of temperatures tested, similar bond strength reductions with temperature were obtained for embedment lengths of 5 and 9 times the diameter of the rebars.

3. Visual observations of the specimens after the tests showed that the damage undergone by the GFRP rebars was limited mostly to their surface, with the superficial layer of sand being completely stripped from the rebars' core; these observations showed that the bond behaviour

538   of the sand-coated GFRP rebars to concrete, at both ambient and elevated temperatures, is

539   influenced by the adhesion (and friction) between the superficial finishing and the rebar's core.

540   4. A numerical method was used to model the behaviour of the GFRP-concrete interface, taking

541   into account the composite nature of these specific rebars; local bond stress *vs.* slip relations

542   were calibrated for different temperatures and allowed reproducing the experimental data in

543   terms of load *vs.* slip response with very high accuracy.

544   5. The empirical models assessed in the present study, proposed by Gibson *et al*. [32] and Correia

545   *et al*. [33], were both able to accurately simulate the GFRP-concrete average bond strength

546   reduction with temperature.

547   The proposed local bond *vs.* slip laws are the main research output of the present study; these

548   relations, which were calibrated for representative sand-coated GFRP rebars and concrete type,

549   can be implemented in the numerical simulation of the thermo-mechanical response of GFRP-RC

550   members (made of similar materials to those adopted in this study) subjected to elevated

551   temperatures or fire.

558   **REFERENCES**

559   [1]   Pradhan B., "Corrosion behavior of steel reinforcement in concrete exposed to composite

560   chloride-sulfate environment", *Construction and Building Materials*, 72, 398–410, 2014.

561   [2]   Benmokrane B., Ali A.H., Mohamed H.M., ElSafty A. and Manalo A., "Laboratory

562   assessment and durability performance of vinyl-ester, polyester, and epoxy glass-FRP bars

563   for concrete structures", *Composites Part B: Engineering*, 114, 163–174, 2017.

564 [3] D'Antino T., Pisani M.A. and Poggi C., "Effect of the environment on the performance of

565 GFRP reinforcing bars", *Composites Part B: Engineering*, 141, 123–136, 2018.

566 [4] Bank L.C., "Composites for Construction - Structural Design with FRP Materials", Wiley,

567 Hoboken, New Jersey, USA, 2006.

568 [5] Mouritz A.P. and Gibson A.G., "Fire Properties of Polymer Composite Materials",

569 Springer, Dordrecht, 2006.

570 [6] Nigro E., Cefarelli G., Bilotta A., Manfredi G. and Cosenza E., "Guidelines for flexural

571 resistance of FRP reinforced concrete slabs and beams in fire", *Composites Part B:*

572 *Engineering*, 58, 103–112, 2014.

573 [7] Katz A., Berman N. and Bank L.C., "Effect of high temperature on bond strength of FRP

574 rebars", *Journal of Composites for Construction*, 3 (2), 73–81, 1999.

575 [8] Carvelli V., Pisani M.A. and Poggi C., "High temperature effects on concrete members

576 reinforced with GFRP rebars", *Composites Part B: Engineering*, 54 (1), 125–132, 2013.

577 [9] Weber A., "Fire-resistance tests on composite rebars", *4th International Conference of*

578 *FRP Composites in Civil Engineering (CICE 2008)*, Zurich, Switzerland, 2008.

579 [10] Abbasi A. and Hogg P.J., "Fire testing of concrete beams with fibre reinforced plastic

580 rebar", *Composites Part A: Applied Science and Manufacturing*, 37 (8), 1142–1150, 2006.

581 [11] Yan F., Lin Z. and Yang M., "Bond mechanism and bond strength of GFRP bars to

582 concrete: a review", *Composites Part B: Engineering*, 98, 56–69, 2016.

583 [12] McIntyre E., Bisby L. and Stratford T., "Bond strength of FRP reinforcement in concrete

584 at elevated temperature", *7th International Conference on FRP Composites in Civil*

585 *Engineering (CICE 2014)*, Vancouver, Canada, 2014.

586 [13] Calvet V., Valcuende M., Benlloch J. and Cánoves J., "Influence of moderate temperatures

587 on the bond between carbon fibre reinforced polymer bars (CFRP) and concrete",

588 *Construction and Building Materials*, 94, 589–604, 2015.

589 [14] Li C., Gao D., Wang Y. and Tang J., "Effect of high temperature on the bond performance

590   between basalt fibre reinforced polymer (BFRP) bars and concrete", *Construction and*

591   *Building Materials*, 141, 44–51, 2017.

592   [15] Hamad R., Johari M.A. and Haddad R., "Mechanical properties and bond characteristics

593   of different fiber reinforced polymer rebars at elevated temperatures", *Construction and*

594   *Building Materials*, 142, 521–535, 2017.

595   [16] Sena-Cruz J. and Barros J., "Modeling of bond between near-surface mounted CFRP

596   laminate strips and concrete", *Computers and Structures*, 82 (17–19), 1513–1521, 2004.

597   [17] Lin X. and Zhang Y.X., "Evaluation of bond stress-slip models for FRP reinforcing bars

598   in concrete", *Composite Structures*, 107 (1), 131–141, 2014.

599   [18] Lin X. and Zhang Y.X., "Nonlinear finite element analyses of steel/FRP-reinforced

600   concrete beams in fire conditions", *Composite Structures*, 97, 277–285, 2013.

601   [19] Rafi M.M. and Nadjai A., "Numerical modelling of carbon fibre-reinforced polymer and

602   hybrid reinforced concrete beams in fire", *Fire and Materials*, 37, 374–390, 2013.

603   [20] Rafi M.M., Nadjai A. and Ali F., "Finite element modeling of carbon fiber-reinforced

604   polymer reinforced concrete beams under elevated temperatures", *ACI Structural Journal*,

605   105 (6), 701–710, 2008.

606   [21] ASTM, "Standard Test Method for Bond Strength of Fiber-Reinforced Polymer Matrix

607   Composite Bars to Concrete by Pullout Testing", ASTM D7913/D7913M-14, *American*

608   *Society for Testing and Materials*, West Conshohocken, Pennsylvania, USA, 2014.

609   [22] ACI Committee 440, "Guide Test Methods for Fiber-Reinforced Polymer (FRP)

610   Composites for Reinforcing or Strengthening Concrete and Masonry Structures", ACI

611   440.3R-12, *American Concrete Institute*, Farmington Hills, Michigan, USA, 2012.

612   [23] Aslan 100, "Glass Fiber Reinforced Polymer (GFRP) Rebar for Infrastructure Solutions,"

613   Technical datasheet - Owens Corning, available at http://aslanfrp.com/resources/Aslan-

614   100-GFRP-Rebar-brochure.pdf.

615   [24] ISO, "Textile-glass-reinforced plastics - Prepregs, moulding compounds and laminates -

616   Determination of the textile-glass and mineral-filler content - Calcination methods", ISO

617   1172, *International Organization for Standardization*, Geneve, Switzerland, 1996.

618   [25]   ASTM, "Standard Test Method for Assignment of the Glass Transition Temperature By

619   Dynamic Mechanical Analysis", ASTM E1640, *American Society for Testing and*

620   *Materials*, West Conshohocken, Pennsylvania, USA, 1999.

621   [26]   ISO, "Fibre-Reinforced Polymer (FRP) Reinforcement of Concrete - Test Methods - Part

622   1: FRP Bars and Grids", ISO 10406-1, *International Organization for Standardization*,

623   Geneve, Switzerland, 2008.

624   [27]   CEN, "Testing Hardened Concrete - Part 3: Compressive Strength of Test Specimens",

625   EN 12390-3, *European Committee for Standardization*, Brussels, Belgium, 2009.

626   [28]   CEN, "Testing Hardened Concrete - Part 3: Tensile Splitting Strength of Test Specimens",

627   EN 12390-6, *European Committee for Standardization*, Brussels, Belgium, 2009.

628   [29]   Sena-Cruz J.M., "Strengthening of concrete structures with near-surface mounted CFRP

629   laminate strips," *PhD thesis in Civil Engineering*, Universidade do Minho, Guimarães,

630   Portugal, 2005.

631   [30]   Eligehausen R., Popov E.P. and Bertero V. V., "Local bond stress-slip relationships of

632   deformed bars under generalized excitations: experimental results and analytical model,"

633   Report No. UCB/EERC-8, Earthquake Engineering Resarch Center, California, USA, 1982.

634   [31]   Stang H. and Aarre T., "Evaluation of crack width in FRC with conventional

635   reinforcement", *Cement and Concrete Composites*, 14 (2), 143–154, 1992.

636   [32]   Gibson A.G., Wu Y.-S., Evans J.T. and Mouritz A.P., "Laminate theory analysis of

637   composites under load in fire", *Journal of Composite Materials*, 40 (7), 639–658, 2006.

638   [33]   Correia J.R., Gomes M.M., Pires J.M. and Branco F.A., "Mechanical behaviour of

639   pultruded glass fibre reinforced polymer composites at elevated temperature: Experiments

640   and model assessment", *Composite Structures*, 98, 303–313, 2013.

641